J. Mech. Phys. Solids Vol. 37, No. 3, pp. 317–350, 1989.
Printed in Great Britain.

0022-5096/89 $3.00 + 0.00

NUMERICAL ANALYSIS OF HYDROGEN TRANSPORT NEAR A BLUNTING CRACK TIP

P. SOFRONIS* and R. M. MCMEEKING†

* Department of Materials Science and Engineering, University of Illinois, 1304 W. Green Street, Urbana, IL 61801, U.S.A.; and † Department of Materials and Department of Mechanical Engineering, University of California, Santa Barbara, CA 93106, U.S.A.

(*Received* 19 *January* 1988; *in revised form* 19 *July* 1988)

ABSTRACT

THE hydrogen transport problem is studied in conjunction with large deformation elastic–plastic behavior of a material. Oriani's equilibrium theory is used to relate the hydrogen in traps (micro-structural defects) to concentration in normal interstitial lattice sites (NILS). The resulting non-linear transient hydrogen diffusion equations are integrated using a modified backward Euler method. Coupled diffusion and plastic straining is analysed with this numerical procedure in the area around a blunting crack tip. A uniform NILS concentration as dictated by Sievert's law at the pressure and temperature of interest is used as initial condition throughout the body. The crack is initially blunted by plane strain mode I (tensile) loading. The finite element results show that hydrogen residing at NILS is generally very small in comparison with the population that develops in trapping sites near the crack surface. That is, lattice diffusion delivers the hydrogen but it is predominantly the trapping that determines its distribution at temperatures of interest. The predominance of trapped hydrogen over lattice concentration prevails even in the case when hydrogen migrates under steady state conditions. Hence, the hydrostatic stress effect is less important than traps created by plastic straining as far as the creation of high total hydrogen concentration is concerned. The trapping site locations and the temperature determine the amounts and locations of high hydrogen concentrations. Consequently, ahead of a blunting crack tip, the total hydrogen concentration and plastic strain diminish with distance from the crack tip whereas the hydrostatic stress rises. This would seem to have significant consequences for fractures induced by the presence of hydrogen.

1. INTRODUCTION

HYDROGEN is a deleterious solute impurity in pure metals and alloys known to be detrimental to almost all systems with regard to their fracture behavior.

Hydrogen embrittlement is not completely understood despite intense investigation over the years (BIRNBAUM, 1979, 1983, 1984; HIRTH, 1980, 1984; LATANISION, 1983; JOHNSON, 1984). It is manifested in various parameters that are used as measures of the mechanical properties of materials such as: elongation to failure; reduction of area; strain hardening rate; tensile strength; fracture toughness; and time to failure. It may also change the mode of fracture from ductile coalescence to brittle intergranular failure. It should be recognized that there is no single mechanism causing hydrogen embrittlement. Rather, it appears that different mechanisms apply to different systems under various conditions. However, it has been established that the interaction of

hydrogen with the lattice and defects in the vicinity of a major crack is generally the basis of the damaging effect (NELSON, 1983; SMIALOWSKI, 1985).

Categorizing hydrogen embrittlement in low hydrogen fugacity environments, one may divide embrittled systems into two broad classes, non-hydride formers and hydride formers. In this work, the behavior of the non-hydride systems is studied. Attention is focused on analysing the solute hydrogen effects as they result from the metal–hydrogen interactions. Phenomena related to the source of hydrogen and the kinetics of entrance into the materials are not considered. Along these lines the literature is reviewed in the following paragraphs from a fracture mechanics viewpoint.

First, JOHNSON *et al.* (1958) and TROIANO (1960) concluded that the phenomenon is controlled by the diffusion of hydrogen into the crack tip region and is strongly influenced by hydrostatic stress gradients. The *decohesion concept* was introduced by STEIGERWALD *et al.* (1960) and TROIANO (1960) to explain fractures caused by hydrogen. The concept was further analysed by ORIANI (1978) and studied on thermodynamic grounds by HIRTH and RICE (1980). The model assumes that high hydrogen concentrations reduce the cohesive bonding force between the metal atoms. However, there is no experimental evidence that hydrogen decreases the cohesive stress. Based on the decohesion concept, models for crack initiation and subsequent crack growth kinetics were proposed by ORIANI and JOSEPHIC (1974, 1977), GERBERICH *et al.* (1974), GERBERICH *et al.* (1976) and GERBERICH (1974). ORIANI and JOSEPHIC related the threshold stress intensity factor for crack initiation to a critical hydrogen concentration on experimental grounds. That concentration was deduced from Sievert's law (ORIANI, 1969; LEE, 1976) and was qualified by the hydrostatic stress elevation (LI *et al.*, 1966). Similar results were found by GERBERICH and co-workers who used linear elastic fracture mechanics in conjunction with basic plasticity ideas. More recently, GERBERICH *et al.* (1987) considered hydrogen trapping at internal material defects in the region of high hydrostatic stress located in from the notch root. Hydrogen trapping was viewed as responsible for high hydrogen concentrations. Crack initiation modeling was based on the decohesion concept. VAN LEEUWEN (1974, 1976) described the stress assisted diffusion of hydrogen towards a crack tip. Based on the critical concentration concept for crack initiation he predicted incubation periods. However, he utilized linear elastic analysis. Similar work was reported by LIU (1970).

The effect of hydrogen on the *plastic behavior* of the materials has been the subject of a long and intense investigation. BEACHEM (1972, 1977) and BERNSTEIN (1974) first introduced the concept of a highly localized plastic rupture mechanism. Hydrogen softening effects were demonstrated more conclusively by MATSUI, KIMURA and MORIYA (1979), MORIYA, MATSUI and KIMURA (1979), MATSUI, KIMURA and KIMURA (1979), KIMURA *et al.* (1981), OGURI and KIMURA (1980), EASTMAN *et al.* (1981, 1982), MATSUMOTO *et al.* (1981), TABATA and BIRNBAUM (1984) and ROBERTSON and BIRNBAUM (1986). Those researchers have carried out extensive studies to determine whether hydrogen reduces the flow stress of various systems such as iron and nickel in a variety of strain rates, temperatures and alloy purities. In contrast to the softening behavior, hardening has been reported by ORIANI (1983) in carbon steels, ASANO and OTSUKA (1976, 1978), ADAIR (1966) and MATSUYAMA *et al.* (1978) in iron.

The effect of hydrogen on the *fracture behavior* is also complex. BERNSTEIN and THOMPSON (1976) and GARBER *et al.* (1976, 1981) studied the fracture behavior of steels having several microstructures. In the case of the hydrogen enhanced plasticity mechanism, ROBERTSON and BIRNBAUM (1986) state that the fractures may be generated by hydrogen induced plastic instability which leads to hydrogen assisted localized ductile rupture processes. LEE *et al.* (1977, 1979a, b) and ONYEWUENYI and HIRTH (1983) found experimentally that the role of hydrogen is to promote plastic instability along characteristic slip lines, thereby enhancing incompatibility stresses and in turn enhancing void nucleation. MORGAN and MCMAHON (1985) discuss an impurity hydrogen embrittlement mechanism which promotes intergranular fracture.

A very important aspect of hydrogen embrittlement is that there exists a *transport stage* of hydrogen to the sites where degradation occur. Hydrogen atoms have to be adsorbed and absorbed by the material. Then, via lattice diffusion or dislocation transport (KURKELA and LATANISION, 1979; DONOVAN, 1976a, b; TIEN *et al.*, 1976; LADNA and BIRNBAUM, 1987; FRANKEL and LATANISION, 1986) hydrogen moves either into the metal lattice or into internal microstructural heterogeneities and defect-traps (ORIANI, 1970; WERT, 1978). BIRNBAUM (1979) points out that concepts like the kinetics of degradation, the ductility dependence on temperature and strain rate, the incubation period and the critical hydrogen concentration build-up before fracture reflect the hydrogen transport kinetics rather than the mechanisms of failure.

Extensive research has illuminated several aspects of the phenomenology thus far (BIRNBAUM, 1985). However, no significant progress has been made in combining analytically the non-linear crack tip mechanical behavior with that of the hydrogen (RICE, 1976, 1977b). Indeed, detailed analysis of the coupling of non-linear diffusion phenomena with elastic–plastic deformation has not been carried out. The only work that has attempted such an analysis is by KITAGAWA and KOJIMA (1983) which is incomplete in several respects. RICE (1976) has pointed out that an accurate analysis treating the hydrogen transport as affected by local stresses and strains is of primary importance towards understanding the phenomenon. Through that analysis, many significant parameters such as the tensile hydrostatic stress assisting diffusion and the trapping effect will be quantified in a precise manner. In this paper, large deformation elastic–plastic analysis (MCMEEKING and RICE, 1975; MCMEEKING, 1977) is coupled with non-linear hydrogen diffusion at a blunting crack tip. An effort is made to include variables known to be significant according to experimental findings. In addition, we try to address some features of the problem to bring out their importance in the embrittlement phenomenon.

2. HYDROGEN TRANSPORT AND PLASTICITY

Hydrogen is considered to move through the materials by normal interstitial lattice site (NILS) diffusion. The dislocation transport mode is neglected in view of the recent studies by LADNA and BIRNBAUM (1987) and FRANKEL and LATANISION (1986) showing that its effect is negligible. The hydrostatic stress induced drift is accounted for. Transported hydrogen resides either at NILS or at trapping sites. The model for trapping is developed in a generalized way without reference to specific types of traps.

At a later state in the modeling, the treatment is made specific by considering evidence of trap site density and occupancy from experiments by KUMNICK and JOHNSON (1980) in pure iron. They believe that traps are associated with the imperfection structure, dislocations and point defect aggregates or dislocation debris. Consequently, the parameter values used in the calculations represent the appropriate mix of microstructural defects acting as traps. Strain rate effects associated with the rate of generation of traps have been allowed for.

(i) *Hydrogen lattice solubility*

Given the type of interstices and the host metal lattice, one can phrase the NILS concentration as follows

$$C_L = \theta_L \beta N_L, \tag{1}$$

where C_L denotes the number of hydrogen atoms per unit lattice volume, β denotes the number of NILS per solvent atom, θ_L denotes the occupancy of the available sites, i.e. θ_L is the ratio of occupied sites to the total available and N_L denotes the number of solvent lattice atoms per unit lattice volume. Parameters β and N_L are fixed for a given lattice. If V_M is the molar volume of the host lattice expressed in units of volume per lattice mole, one can write

$$N_L = \frac{N_A}{V_M}, \tag{2}$$

where $N_A = 6.0232 \times 10^{23}$ atoms per mole is Avogadro's number.

(ii) *Trapping*

The hydrogen concentration at traps can be written as

$$C_T = \theta_T \alpha N_T, \tag{3}$$

where C_T denotes the number of trapped hydrogen atoms per unit lattice volume, α denotes the number of hydrogen atom sites per trap, θ_T denotes the occupancy of the available sites, i.e. θ_T is the ratio of occupied sites to the total available, and N_T denotes the number of traps per unit lattice volume.

Trap behavior can be modeled according to the formulations presented by ORIANI (1970) and MCNABB and FOSTER (1963). In this paper, ORIANI's approach is adopted while a related numerical treatment based on the McNabb and Foster theory can be found in the dissertation by SOFRONIS (1987). It is worth mentioning that most prior numerical treatments of the hydrogen transport problem are based on the McNabb and Foster formulation although notable exceptions are ELLERBROCK *et al.* (1972) and ALLEN-BOOTH *et al.* (1975). However, SOFRONIS (1987) has demonstrated that in the circumstances relevant to the work described in this paper there is little difference in the results between the two formulations.

Oriani's theory assumes local equilibrium between H in reversible traps and lattice

sites. It can be used when the trap filling kinetics are very rapid as is usually the case. Assuming that both lattice and trap sites constitute finite populations and furthermore assuming no interactions between occupied sites, one may write

$$\frac{1-\theta_L}{\theta_L}\frac{\theta_T}{1-\theta_T} = K. \tag{4}$$

In (4) K represents equilibrium between lattice and trap sites and is given by

$$K = \exp\left(-\frac{\overline{\Delta H}_B}{RT}\right), \tag{5}$$

where $\overline{\Delta H}_B$ is the trap binding energy, inherently negative, R is the gas constant equal to 8.3144 J mol^{-1} K^{-1} and T is the absolute temperature. In the case of low NILS concentrations C_L, i.e.

$$\theta_L \ll 1, \tag{6}$$

by using (1), (3) and (4), one finds

$$C_T = \frac{K\frac{\alpha N_T}{\beta N_L}C_L}{1+\frac{K}{\beta N_L}C_L}, \tag{7}$$

which characterizes the equilibrium relationship between C_L and C_T in terms of material parameters. Thus, as temperature is increased and K decreases, the concentration of hydrogen in traps will reduce when C_L is held fixed. Finally, some insight into the process of equilibrium trap-filling at fixed temperature and N_T can be obtained by the differentiation of (7). This gives

$$\frac{\partial C_T}{\partial C_L} = \frac{C_T(1-\theta_T)}{C_L}. \tag{8}$$

Thus, the fractional change of trapping site concentration is proportional to the fractional change of the NILS concentration C_L and to the unoccupied proportion of traps.

(iii) *Hydrogen lattice diffusion*

Chemical potential gradients constitute the driving force for this diffusion. At low concentrations, at which there is no interaction between the diffusing species and the rate of diffusion depends only on hydrogen mobility (KEDZIERZAWSKI, 1985), one can relate the hydrogen flux $\mathbf{J}$ to the gradient of the chemical potential μ as follows

$$\mathbf{J} = -\frac{DC_L}{RT}\nabla\mu, \tag{9}$$

where D is the lattice diffusion constant that is assumed to be independent of stress.

In general, for a system under external stress and in conditions in which (9) is valid, we can write at constant pressure and temperature

$$\mu = \mu^0 + RT \ln C_L + \mu_\sigma, \tag{10}$$

where μ^0 is the chemical potential in the "standard state" and μ_σ is the stress dependent part of μ. Substituting (10) into (9), we find

$$\mathbf{J} = -D\nabla C_L - \frac{DC_L}{RT}\nabla\mu_\sigma. \tag{11}$$

Assuming that NILS hydrogen causes only dilational distortion to the lattice, one can write (LI *et al.*, 1966)

$$\mu_\sigma = -\frac{\sigma_{kk}}{3}\bar{V}_H, \tag{12}$$

where σ_{ij} is the externally applied stress, $\bar{V}_H$† is the partial molar volume of hydrogen in solid solution, and the repeated index summation convention is used. The assumption of dilational distortion is known to be correct to a first order approximation (HIRTH, 1977). Integrating (11) when $\mathbf{J} = 0$ and using formula (12) for μ_σ, we obtain the steady state concentration in a stressed lattice as

$$\frac{C_L^\sigma}{C_L^0} = \exp\left(\frac{\sigma_{kk}\bar{V}_H}{3RT}\right), \tag{13}$$

where C_L^0 is the concentration in the absence of stress. Thus if T is increased finitely while $\sigma_{kk} > 0$ and C_L^0 are held fixed, the steady concentration of hydrogen will diminish.

Next, we proceed to formulate the *hydrogen diffusion initial value problem*. Let us consider an arbitrary volume V of material bounded by a surface S at a given temperature T and subject to external loading σ_{ij}. Hydrogen resides inside V, either in NILS (C_L) or in trapping sites (C_T). The two populations are assumed to be constantly in equilibrium as described by (7). Any change of hydrogen concentrations C_L and C_T in V is accompanied by hydrogen flux through S. Mass conservation requires that the rate of change of total hydrogen ($C_L + C_T$) inside V be equal to the flux through S. Therefore the continuity equation is written as follows

$$\frac{\mathrm{d}}{\mathrm{d}t}\int_V (C_L + C_T)\,\mathrm{d}V + \int_S \mathbf{J}\cdot\mathbf{n}\,\mathrm{d}S = 0, \tag{14}$$

where $\mathbf{n}$ is the outward unit surface normal vector and $\mathrm{d}/\mathrm{d}t$ is the time derivative. We assume that at any time t the deformations of the body shape do not affect diffusion substantially. Replacing $\mathbf{J}$ in (14) as given by (11), using the divergence theorem and by means of the arbitrariness of volume V we find

† An overbar ($\bar{}$) denotes partial molar quantity.

$$\frac{dC_L}{dt} + \frac{dC_T}{dt} = DC_{L,ii} + \left(\frac{DC_L}{RT}\mu_{\sigma,i}\right)_{,i}, \tag{15}$$

where $(\ )_{,i} = \partial(\ )/\partial x_i$. Next, using Oriani's equilibrium theory one may phrase the left hand side of (15) in terms of C_L. Considering that

$$\frac{dC_T}{dt} = \frac{\partial C_T}{\partial C_L} \cdot \frac{dC_L}{dt}$$

at fixed temperature T and deformation levels N_T, one has by means of (8)

$$\frac{D}{D_{\text{eff}}}\frac{dC_L}{dt} = DC_{L,ii} + \left(\frac{DC_L}{RT}\mu_{\sigma,i}\right)_{,i}, \tag{16}$$

where the effective diffusion constant is given by

$$D_{\text{eff}} = D\frac{C_L}{C_L + C_T(1-\theta_T)} \quad \text{for} \quad \theta_L \ll 1 \tag{17}$$

under the assumption (6). Partial differential equation (16) can be solved in a closed region V provided that initial conditions are given and the value of C_L or its normal derivative $\partial C_L/\partial \mathbf{n}$ or a linear combination of C_L and $\partial C_L/\partial \mathbf{n}$ are prescribed at every point of the boundary S. It should be noted that a drift term which results in the Laplacian of σ_{kk} is included, provided that the stress dependent part μ_σ of the chemical potential μ is given by (12). Analyses done by others so far did not include $\sigma_{kk,ii}$ because plane strain linear elasticity was assumed.

We continue by formulating the *finite strain elastic–plastic boundary value problem.* The material is assumed initially homogeneous and isotropic. In the plastic regime it hardens isotropically and flows according to von Mises J_2 flow theory. In the case of finite deformations, the associated flow law is provided by the classical Prandtl–Reuss equations modified by McMeeking and Rice (1975)

$$\overset{\nabla}{\tau}_{ij} = 2G\left[\delta_{ik}\delta_{jl} + \frac{\nu}{1-2\nu}\delta_{ij}\delta_{kl} - \frac{3}{2}\frac{\tau'_{ij}\tau'_{kl}}{\left(\frac{h}{3G}+1\right)\bar{\tau}^2}\right]D_{kl} \tag{18}$$

for plastic loading and

$$\overset{\nabla}{\tau}_{ij} = 2G\left(\delta_{ik}\delta_{jl} + \frac{\nu}{1-2\nu}\delta_{ij}\delta_{kl}\right)D_{kl}$$

for elastic loading or any unloading, where τ is a stress measure (Kirchhoff stress) defined as

$$\boldsymbol{\tau} = J^0\boldsymbol{\sigma},$$

$\boldsymbol{\sigma}$ is the Cauchy stress, J^0 is the ratio of the density of the material in the stress free state (ρ^0) to the density of the material in the current state (ρ), $\mathbf{D}$ is the deformation rate tensor and equals the symmetric part of the velocity gradient in spatial coordinates, δ_{ij} is the Kronecker delta, τ'_{ij} is the deviatoric part of the stress tensor τ_{ij}

$$\tau'_{ij} = \tau_{ij} - \tfrac{1}{3}\tau_{kk}\,\delta_{ij}.$$

$\bar{\tau}$ is the equivalent stress defined by

$$\bar{\tau}^2 = \tfrac{3}{2}\tau'_{ij}\tau'_{ij}.$$

G and ν are the shear modulus and Poisson's ratio respectively and h is the slope of the uniaxial Kirchhoff stress versus logarithmic plastic strain

$$h = \frac{\mathrm{d}\bar{\tau}}{\mathrm{d}\bar{\varepsilon}^p}.$$

In multiaxial deformation $\bar{\varepsilon}^p$ is defined as

$$\bar{\varepsilon}^p = \int \sqrt{\tfrac{2}{3}D^p_{ij}D^p_{ij}}\,\mathrm{d}t,$$

where $\mathbf{D}^p$ is the plastic part of the deformation rate expressed as $\mathbf{D} = \mathbf{D}^e + \mathbf{D}^p$ with $\mathbf{D}^e$ denoting the elastic part. Finally, the superposed ∇ denotes the Jaumann or co-rotational stress rate which exhibits proper material invariance for rigid spin.

The governing equations of rate equilibrium accounting for changes of the deformed volume of the material are cited by MCMEEKING and RICE (1975) in the form of a variational statement. If V is the volume of the material in the current configuration bounded by the surface S the variational statement has the form

$$\int_V (\overset{\nabla}{\sigma}_{ij} + D_{kk}\sigma_{ij})\,\delta D_{ij}\,\mathrm{d}V - \int_V \tfrac{1}{2}\sigma_{ij}\,\delta(2D_{ik}D_{kj} - v_{k,i}v_{k,j})\,\mathrm{d}V$$

$$= \int_S \dot{T}_i\,\delta v_i\,\mathrm{d}S + \int_V \dot{b}_i\,\delta v_i\,\mathrm{d}V, \quad (19)$$

where

$$\overset{\nabla}{\sigma}_{ij} + D_{kk}\sigma_{ij} = \frac{1}{J}\overset{\nabla}{\tau}_{ij}.$$

$\mathbf{T}$ is the traction vector which is specified on the part S_T of the surface S where tractions are prescribed and $\mathbf{b}$ is the body force per unit volume in the reference configuration. Note that $\dot{\mathbf{T}}$ and $\dot{\mathbf{b}}$ are nominal rates of change (MCMEEKING and RICE, 1975). The symbol δ indicates an arbitrary virtual variation of the quantity it precedes. Any virtual velocity variations are constrained to vanish on the part S–S_T of the surface where velocities are prescribed.

3. COUPLING OF THE INITIAL VALUE HYDROGEN DIFFUSION PROBLEM WITH THE ELASTIC–PLASTIC BOUNDARY VALUE PROBLEM AT A BLUNTING CRACK TIP

In this work, hydrogen diffusion is affected by hydrostatic stress and by plastic straining through trapping. The hydrogen effects on the elastic–plastic behavior are not taken into consideration since they will be treated in subsequent work. The

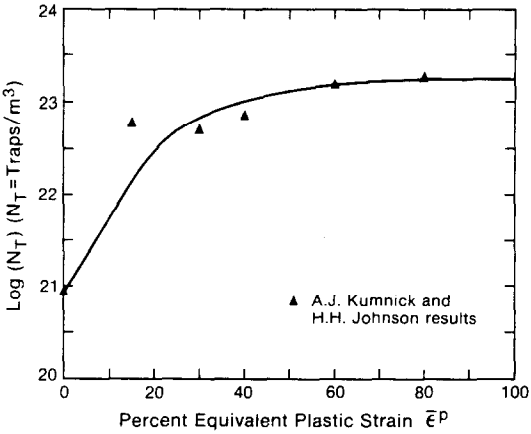

FIG. 1. A proposed relationship between the trap density N_T and the equivalent plastic strain $\bar{\varepsilon}^p$ for iron.

analysis is carried out for a BCC iron system with an initially blunted crack tip. Trap characteristics of this sytem are fairly well established (KUMNICK and JOHNSON, 1980). They found that the trap binding energy is $\overline{\Delta H}_B = -60$ kJ mol^{-1} independent of the temperature and the amount of plastic deformation. They found also that trap densities are independent of temperature, increase sharply with deformation at low deformation levels and then more gradually with further deformation. In accord with these experimental observations we assumed that the trap density N_T varies with equivalent plastic strain $\bar{\varepsilon}^p$ as shown in Fig. 1. Notice that the density is assumed to saturate at plastic strains greater than 80%. The parameter α in (3) was taken to be equal to 1. The parameter β in (1) was taken equal to 6 with tetrahedral site occupancy assumed (HIRTH, 1980; WANG *et al.*, 1985; PIERCY, 1978) despite arguments favoring octahedral occupancy (STURGES and MIODOWNIK, 1969; SAKAMOTO *et al.*, 1985). The molar volume of iron is $V_M = 7.116 \times 10^{-6}$ m^3 mol^{-1} (METALS HANDBOOK, 1985). Hence, (2) furnishes $N_L = 8.4643 \times 10^{28}$ solvent lattice atoms per cubic meter. Interstitial hydrogen is assumed to expand the lattice isotropically and its partial molar volume in solution is $\bar{V}_H = 2.0 \times 10^{-6}$ m^3 mol^{-1} (HIRTH, 1980). According to VÖLKL and ALEFELD (1978) a good estimation of the diffusion constant D is given by

$$D = 2.10 \times 10^{-7} \frac{m^2}{S} \exp\left(-\frac{6.88 \text{ kJ mol}^{-1}}{RT}\right) \tag{20}$$

at temperatures greater than 325 K. The hydrogen stress free equilibrium solubility as a function of environmental pressure and temperature is given by Sievert's law for temperatures well above 300 K (JOHNSON, 1974) as

$$C_L = 1.989 \times 10^{26} \sqrt{p} \exp\left(-\frac{\overline{\Delta H}_S}{RT}\right), \tag{21}$$

where C_L is atoms of H_2 gas (under normal conditions of pressure and temperature) per m^3 of iron, p is the hydrogen pressure in atmospheres and $\overline{\Delta H}_S = 28.6$ kJ mol^{-1} (HIRTH, 1980) is the heat of solution.

The modeling applies to both environmental and internal embrittlement. In the case of environmental embrittlement, the annealed specimen is assumed to be at a given temperature T and surrounded by gaseous hydrogen of the same temperature at pressure p. At time zero the stress-free solid is in equilibrium with the hydrogen gas and uniform NILS concentrations, $C_L = C_0$ given by Sievert's law, have been established everywhere. Trapping site concentrations C_T follow from the NILS population through (7). If the crack surface is assumed to be insulated at $t > 0$, hydrogen diffusion in the solid dominates the transport phenomena. If the crack interface is "open" to allow equilibration with the hydrogen gas, the dominant process is hydrogen transport from the crack tip.

In the case of internal embrittlement, at time zero hydrogen is in NILS and trapping sites, the two populations $C_L = C_0$ and C_T being in equilibrium at a given temperature T as (7) dictates. The material is annealed and all external surfaces including those of the crack are assumed to be insulated. Such a specimen is obtained via cathodic or thermal charging followed by insulation of its surfaces to preclude hydrogen loss.

At time zero loads are applied, and subsequently increased to levels where the size of the crack opening displacement is increased to several times its initial size. The plastic response of the material is assumed to be rate independent and consequently the load increments may be chosen relative to the diffusion time as desired.

We are interested in plane strain local yielding situations where the plastic zone is confined in an area about the crack tip whose size is negligible compared with any dimensions of the specimen. In this way small scale yielding conditions are enforced. Therefore, as RICE (1968a) points out, the boundary layer approach is valid with the finite geometry material replaced by an infinite body with a semi-infinite crack and asymptotic boundary conditions of the IRWIN (1960) singular linear elastic field replacing the actual conditions at a remote boundary. Those conditions are applied incrementally for mode I (tensile) opening and are of the form

$$u_i = \frac{K_I}{2G}\sqrt{\frac{r}{2\pi}}\, f_i(\nu, \theta) \quad \text{as} \quad r \to \infty, \tag{22}$$

where u_i with $i = x, y$ is the displacement, K_I is the stress intensity factor from the solution of the linear elastic crack problem, r and θ are polar coordinates as in Fig. 2 and f_i is the universal function for plane strain independent of geometry and load (RICE, 1968b). The crack surface is assumed traction free.

Symmetry allows modeling both the diffusion and elastic–plastic behavior in the 2-dimensional region $0 \leqslant \theta \leqslant \pi$ (see Fig. 2). Thus, the symmetry line $\theta = 0$ is free of shear tractions and displacements in the y direction. Hydrogen flux across the symmetry line $\theta = 0$ is zero.

4. NUMERICAL FORMULATION OF THE HYDROGEN TRANSPORT PROBLEM

In this section the numerical methods used to solve the problems described in the preceding section are developed.

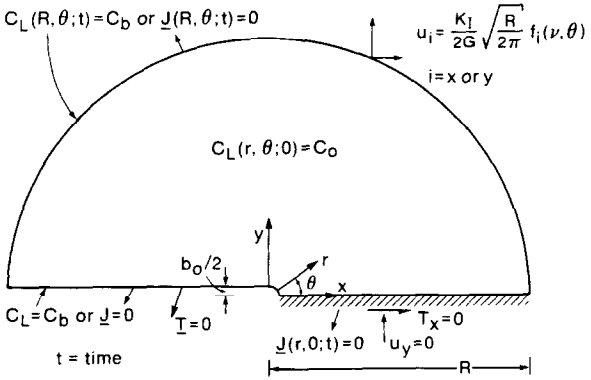

FIG. 2. Description of the boundary and initial conditions for the coupled diffusion and elastic–plastic problems under small scale yielding conditions. Constants C_b and C_0 are given concentrations C_L in NILS, **J** is hydrogen vector, **u** displacement and **T** traction.

(i) *Variational description of the diffusion initial value problem*

We consider the initial value problem described by (16) in a volume V bounded by a surface S. Surface S consists of parts S_C where

$$C_L = C_b, \tag{23}$$

where C_b is a given concentration, and S_N, where

$$-D\left(\mathbf{n}\cdot\nabla C_L + \frac{C_L}{RT}\mathbf{n}\cdot\nabla\mu_\sigma\right) = \phi, \tag{24}$$

in which ϕ is prescribed flux. Surfaces S_C and S_N are such that $S_C \cup S_N = S$. In addition

$$C_L = C_0 \tag{25}$$

throughout V at time zero, where C_0 is a known concentration. For any variation of C_L such that

$$\delta C_L = 0 \quad \text{on} \quad S_C, \tag{26}$$

by means of (12) and (16) we can write at any instant of time t

$$-\int_V \delta C_{L,i} C_{L,i}\,\mathrm{d}V - \frac{1}{D}\int_{S_N}\delta C_L\phi\,\mathrm{d}S + \int_V \delta C_{L,i}\frac{\bar{V}_H}{3RT}C_L\sigma_{kk,i}\,\mathrm{d}V = \int_V \delta C_L\frac{1}{D_{\text{eff}}}\frac{\partial C_L}{\partial t}\,\mathrm{d}V. \tag{27}$$

(ii) *Finite element formulation of the diffusion initial value problem*

The finite element method is used to solve the diffusion initial value problem as stated in its "weak formulation" by (27). The continuum is discretized in the standard

fashion into a finite element mesh. By means of the variational statement (27) we deduce finite element equations

$$[M]\{\dot{C}_L^N\} + [K]\{C_L^N\} = \{F\}, \tag{28}$$

where $[M]$ is the concentration capacity matrix, given by

$$[M] = \int_V [A]^T \frac{1}{D_{\text{eff}}} [A] \, \mathrm{d}V,$$

$[K]$ is the diffusivity matrix, given by

$$[K] = [K_1] + [K_2]$$

with

$$[K_1] = \int_V [B]^T [B] \, \mathrm{d}V,$$

$$[K_2] = -\int_V [B]^T \frac{\bar{V}_H}{3RT} [B]\{\sigma^N\}[A] \, \mathrm{d}V,$$

$\{F\}$ is the diffusion flux vector, given by

$$\{F\} = -\frac{1}{D} \int_{S_\sigma} [A]^T \phi \, \mathrm{d}S$$

and $\{C_L^N\}$ is the array of nodal values of C_L. $[A]$ and $[B]$ are the interpolation matrices such that

$$C_L = [A]\{C_L^N\}$$

and $\{C_{L,x} C_{L,y}\}^T = [B]\{C_L^N\}$. The array $\{\sigma^N\}$ contains values for σ_{kk} at each node and this is also interpolated by the matrix $[A]$. Evidently, Eqs (28) are nonlinear because matrix $[M]$ depends on the NILS concentration C_L and the trapping site concentration C_T through the effective diffusion constant D_{eff}. Also, the matrix $[K]$ depends on the hydrostatic stresses σ_{kk} which are furnished by the elastic–plastic analysis.

(iii) *Numerical integration of the equations*

For convenience, we rewrite Eqs (28) so that the diffusivity matrix becomes symmetric:

$$[M]\{\dot{C}_L^N\} + [K_1]\{C_L^N\} = \{R\}, \tag{29}$$

where

$$\{R\} = \{F\} - [K_2]\{C_L^N\}.$$

Since matrix $[M]$ and array $\{R\}$ are dependent on the current $\{C_L^N\}$, a simple extrapolation can be used, with the values of $[M]$ and $\{R\}$ taken from the previous step

$$[M]_{t+\Delta t} = [M]_t \quad \text{and} \quad \{R\}_{t+\Delta t} = \{R\}_t. \tag{30}$$

CULHAM and VARGA (1971) used such a scheme for the solution of a system of equations similar to (28). We assumed also, that as far as the diffusion equations are concerned, hydrostatic stresses do not vary within a step allowing the use of $\{R\}_{t+\Delta t} = \{R\}_t$. A modified backward Euler method was developed based on the Eqs (29) at time $t+\Delta t$. Equations (30) were used to replace the unknown matrices $[M]_{t+\Delta t}$ and $\{R\}_{t+\Delta t}$ in Eqs (29). The time derivatives are written

$$\{\dot{C}_L^N\}_{t+\Delta t} = \frac{1}{\Delta t}(\{C_L^N\}_{t+\Delta t} - \{C_L^N\})$$

and the final result is

$$\left[\frac{1}{\Delta t}[M]_t + [K_1]\right]\{C_L^N\}_{t+\Delta t} = \frac{1}{\Delta t}[M]_t\{C_L^N\}_t + \{F\}_t - [K_2]_t\{C_L^N\}_t. \tag{31}$$

From a known $\{C_L^N\}$ at $t = 0$, Eqs (31) yield $\{C_L^N\}_{\Delta t}$. Then using $\{C_L^N\}_{\Delta t}$ we find $\{C_L^N\}_{2\Delta t}$ and so on. The scheme is noniterative within each step, and this is more stable than iterative backward Euler schemes as noted by ZIENKIEWICZ (1977) and confirmed by us in numerical experiments using Eqs (29).

We found also that oscillations occur when we initiated the system using a zero initial concentration ($C_0 = 0$) and boundary concentrations (C_b) of the order of 10^{21} atoms of hydrogen per m^3. The oscillations seem to be due to steep concentration gradients which occur initially at the boundary (ZIENKIEWICZ, 1977). The simultaneous reduction of both element size and time step is necessary to avoid this difficulty. In crack tip problems, finely discretized near tip fields and coarsely discretized far fields for cost reduction may contribute to the oscillatory problems. Equal element size throughout the body is desirable, but with the mesh becoming fine at areas which can have steep concentration gradients such as at boundaries. To alleviate the difficulty, we chose instead to solve problems with an initial concentration equal to the boundary concentration ($C_b = C_0$). In addition, our experience with the model shows that stability and accuracy assessments of an algorithm for the solution of linear systems do not guarantee that the algorithm will behave well in non-linear problems.

(iv) *Numerical integration of the elastic–plastic boundary value problem equations*

The finite element equations were derived from the variational statement (19) based on the updated Lagrangian formulation of MCMEEKING and RICE (1975). This was modified to allow for near incompressible material response (NAGTEGAAL *et al.*, 1974). The analysis was plane strain and constitutive Eqs (18) were integrated by the backward Euler method (ORTIZ and POPOV, 1985).

(v) *Description of the coupled numerical scheme*

At *time zero* nodal lattice concentrations $\{C_L^N\}_0$ and trap concentrations $\{C_T^N\}_0$ are given as described in the previous section and the material is undeformed. Loads are

applied which elastically strain the most highly stressed point to yield. At that stage, an elastic solution for the hydrostatic stress $\frac{1}{3}\sigma_{kk}$ is known. These hydrostatic stresses are used to compute the stiffness matrix $[K_2]_0$ in (31). The trap density for zero plastic strain is used to compute the quantities θ_L, θ_T and D_{eff} by (1), (3) and (17) respectively. Then the matrix $[M]_0$ is computed in (31) which is subsequently solved for $\{C_L^N\}_{\Delta t}$ with $\{F\}_0$ equal to zero. Trap concentrations $\{C_T^N\}_{\Delta t}$ at the nodes are then found via (7). Thus, stresses σ_{kk}, plastic strains $\bar{\varepsilon}^p$ and concentrations C_L, C_T are known at *time* Δt. Loads are then incremented and the elastic–plastic boundary value problem is solved again furnishing $(\sigma_{kk})_{2\Delta t}$ and $(\bar{\varepsilon}^p)_{2\Delta t}$ since plastic straining will now occur. Matrices $[K_2]_{\Delta t}$ and $[M]_{\Delta t}$ are formulated and solutions for $\{C_L^N\}_{2\Delta t}$ and $\{C_T^N\}_{2\Delta t}$ are found. Subsequently evolution of the process takes place in the same way as between times Δt and $2\Delta t$.

(vi) *The finite element mesh*

In Fig. 3(a) the finite element mesh that was used in the near tip region is shown in its undeformed configuration. This mesh was surrounded by the mesh shown in Fig. 3(b), which was surrounded in turn by that shown in Fig. 3(c). The mesh in Fig. 3(d) is the outermost segment. A total of 939 4-noded quadrilateral isoparametric elements was used with 1007 nodes. Exactly the same mesh was used for both the diffusion and the elastic–plastic problem. The concentration capacity matrix $[M]$, diffusivity matrix $[K]$ and elastic–plastic stiffness matrix $[K]$ were integrated by means of a 2×2 gaussian rule in each element. The initial crack width is designated b_0 (see Fig. 2) and the ratio of the radius R of the outer periphery (see Fig. 2) to the radius of the initial notch root $(b_0/2)$ is 30,000. Displacement boundary conditions were applied at this outer radius according to (22). By applying the boundary conditions so remotely from the crack tip, we could enforce small-scale yielding conditions quite easily. Indeed, in all cases, the far field was dominated by the linear elastic stress field. Very fine discretization of the region near the crack tip was used for accurate modeling of the crack tip blunting and of the plasticity effects on the diffusion of hydrogen.

5. RESULTS

Two series of computations were carried out with regard to the material's mechanical properties. In the first, the yield stress in uniaxial tension, σ_0, was equal to 250 MPa. This case is relevant to impure iron. In the second, σ_0 was taken equal to 1200 MPa, a value which characterizes high strength steels. Poisson's ratio ν was 0.3 and Young's modulus E was 207 GPa. The uniaxial stress–strain law was given by a power-law hardening relationship of the form

$$\left(\frac{\bar{\tau}}{\sigma_0}\right)^{1/N} = \frac{\bar{\tau}}{\sigma_0} + \frac{3G}{\sigma_0}\bar{\varepsilon}^p,$$

where $N = 0.2$.

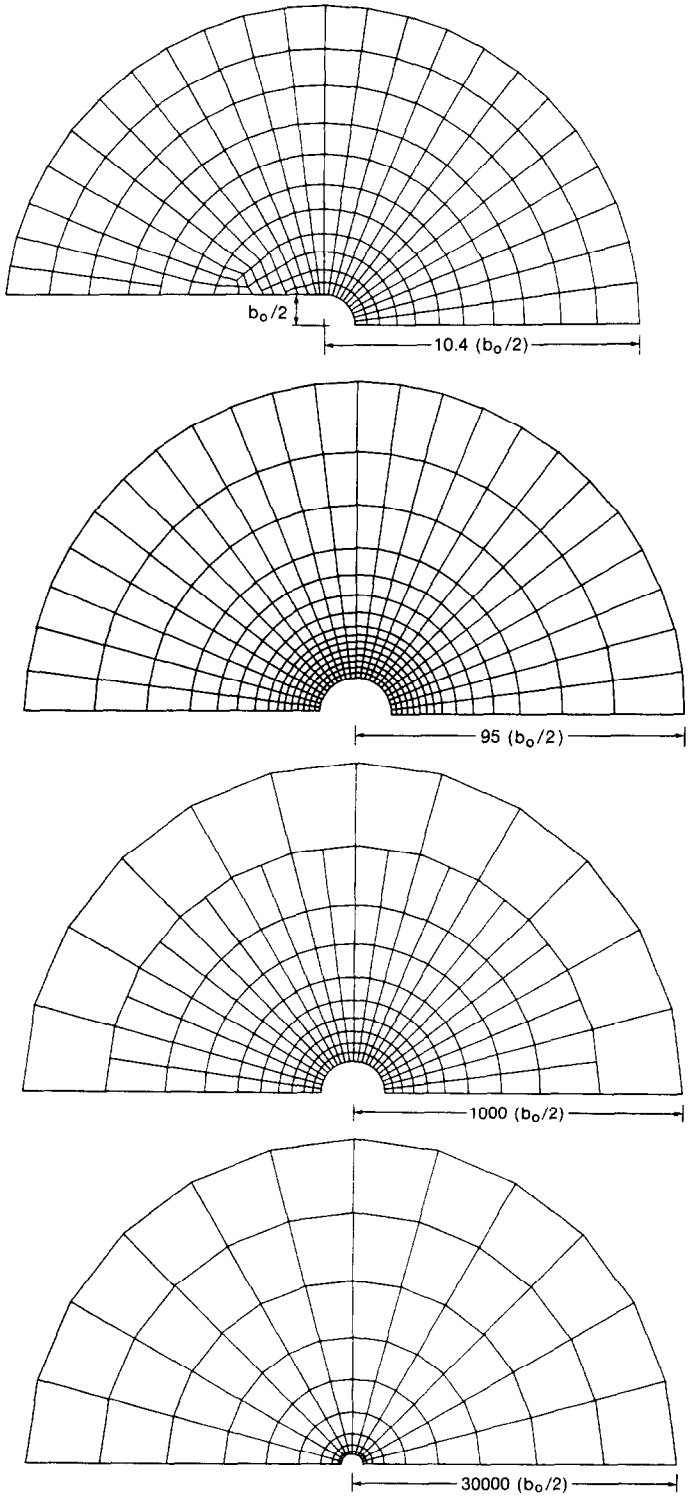

FIG. 3. (a) Near tip region finite element mesh. (b) Finite element mesh surrounding that of (a). (c) Finite element mesh surrounding that of (b). (d) Finite element mesh surrounding that of (c).

The system was at a temperature of 300 K in the case of impure iron and at 150 K for high strength steel. The pressure of the environmental hydrogen was 1 atm. Consequently, the boundary (C_b) and initial NILS concentrations (C_0) (23, 25) were furnished by (21) as being equal to 2.084×10^{21} hydrogen atoms per cubic meter of metal lattice for iron and 2.184×10^{16} atoms per cubic meter for steel. Lattice diffusion constants were 1.27×10^{-8} m^2 s^{-1} for iron and 8.04×10^{-8} m^2 s^{-1} for steel according to (20).

The first increment of load was such that it just caused yielding at the most severely stressed material element. Subsequently, the applied stress intensity factor was increased in each step by half of that of the first step. Solutions of the hydrogen diffusion equations were obtained when plastic deformation was occurring with time steps equal to 0.5 s. Such steps, small compared to the long times characterizing the embrittlement phenomena, were required for numerical accuracy and stability. However, at fixed load and thus when no further plasticity was occurring, a much larger time step could be utilized due to the fact that the matrix coefficients of the finite element Eqs (29) did not change substantially with time. The crack opening displacement b_0 in the undeformed configuration of the body was taken equal to 10 μm, a dimension relevant to a prefatigued crack in a material.

Before discussing the results, we note that they are substantially independent of hydrogen flux boundary conditions. Thus, we discuss only the case where all external surfaces, including that of the crack are at a fixed NILS concentration C_L.

(i) *Results relevant to impure iron* ($\sigma_0 = 250$ MPa)

The load was increased from zero at a rate of 0.69 MPa $\sqrt{m}$ s^{-1} for 130 s. After 130 s, K was held fixed. At this stage the crack tip opening displacement was approximately 5 times the initial value. In Fig. 4 the equivalent plastic strain $\bar{\varepsilon}^p$ prevailing at 130 s is plotted against the distance R from the notch root in the

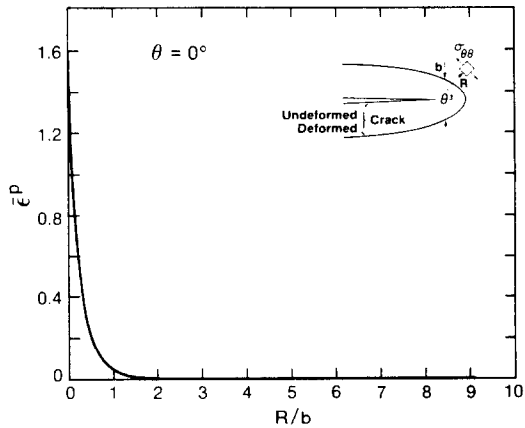

FIG. 4. Plot of equivalent plastic strain $\bar{\varepsilon}^p$ vs distance R/b for impure iron ($\sigma_0 = 250$ MPa) after 130 s when the crack opening displacement b equals $5b_0$.

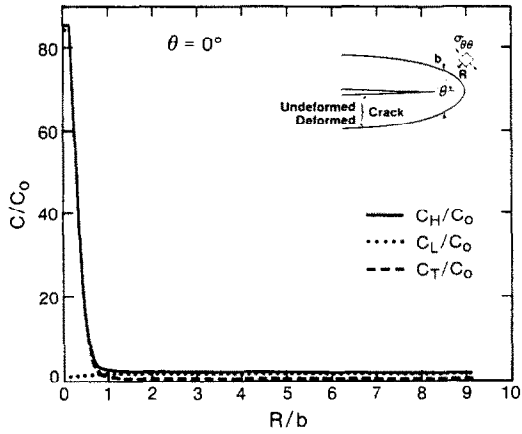

FIG. 5. Plot of hydrogen concentration C_L/C_0 in normal interstitial lattice sites (NILS). C_T/C_0 in trapping sites and C_H/C_0 ($C_H = C_L + C_T$) vs distance R/b for impure iron ($\sigma_0 = 250$ MPa) after 130 s when the crack opening displacement b equals $5b_0$. Nominal concentration C_0 equals 2.084×10^{21} hydrogen atoms m^{-3}.

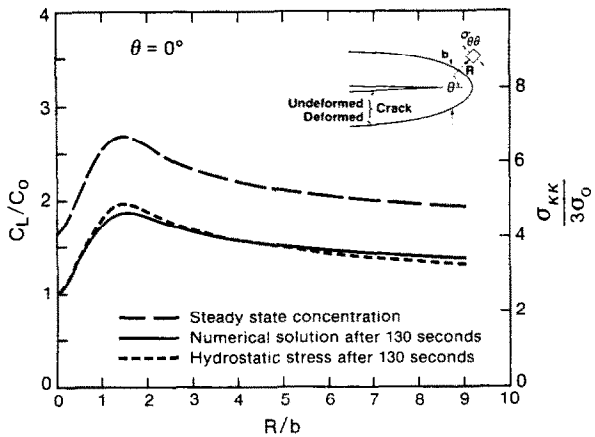

FIG. 6. Plot of hydrogen concentration C_L/C_0 in NILS, hydrostatic stress $\sigma_{kk}/3\sigma_0$ and corresponding steady state concentration vs distance R/b for impure iron ($\sigma_0 = 250$ MPa) after 130 s when the crack opening displacement b equals $5b_0$.

undeformed configuration for $\theta = 0$. Distance R is normalized by the current crack opening displacement b.

Figures 5 through 9 show parameters related to hydrogen on the axis of symmetry ($\theta = 0$) ahead of the notch tip at time $t = 130$ s when $b \simeq 5b_0$. In Fig. 5 the hydrogen concentrations $C_H = C_L + C_T$, C_L and C_T are plotted against R/b. Concentrations C_H, C_L and C_T are normalized by the nominal concentration C_0. Concentration C_L is plotted on an expanded scale against distance R/b in Fig. 6. On the same figure, both the hydrostatic stress $\frac{1}{3}\sigma_{kk}$ and the corresponding steady state concentration based on (13) are also plotted. It can be seen that all three curves attain their maxima at $R/b = 1.53$. This is a consequence of the aspect of the model that NILS hydrogen

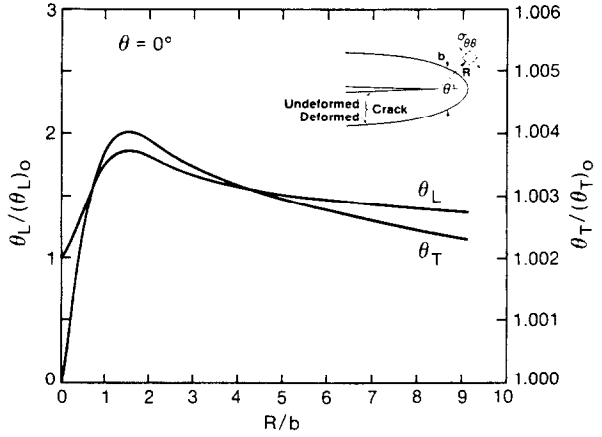

FIG. 7. Plot of NILS trapping site occupancies $\theta_L/(\theta_L)_0$ and $(\theta_T)/(\theta_T)_0$ respectively vs distance R/b for impure iron ($\sigma_0 = 250$ MPa) after 130 s when the crack opening displacement b equals $5b_0$. Constants $(\theta_L)_0$ and $(\theta_T)_0$ equal to 4.103×10^{-9} and 0.9914 respectively.

tends to diffuse towards the region with the largest tensile hydrostatic stress. Also, the numerically computed values of C_L are well below the values for steady state.

In Fig. 7 the occupancies θ_L and θ_T are shown vs distance R/b. Occupancies $(\theta_L)_0$ and $(\theta_T)_0$ at time $t = 0$ were used as normalizing quantities, with $(\theta_L)_0$ computed via the formula (1) with C_L taken to be equal to the nominal concentration C_0. The value of $(\theta_L)_0$ is 4.103×10^{-9}. Then, formulae (4) and (6) furnish a value of $(\theta_T)_0$ equal to 0.9914. Both $\theta_L/(\theta_L)_0$ and $\theta_T/(\theta_T)_0$ are equal to 1 at $R/b = 0$ because that point is a boundary for the NILS concentration C_L. As can be seen in Fig. 7, the occupancy θ_L varies with R/b in a manner similar to C_L. This is a consequence of formula (1). The occupancy θ_T varies similarly to occupancy θ_L because (4) and (6) yield θ_T as a monotonically increasing function of θ_L at fixed temperature. NILS are sparingly occupied and the occupancies θ_L are of the order of 10^{-9}. This is due to the temperature at which the calculations were carried out. Indeed we have seen that the nominal concentration C_0 is equal to 2.084×10^{21} atoms m^{-3}. Figure 6 shows that the concentration C_L rises to no more than twice this. Hence (1) determines occupancies θ_L which are less than 8.2×10^{-9}. The same point is used to explain why traps are almost completely filled with their occupancies θ_T being equal approximately to 0.99. Equation (5) yields a value of 2.8×10^{10} for the equilibrium constant K. Then, θ_T is close to 1 since $K\theta_L$ is of the order of 10^2. Note that when $K\theta_L$ is larger than 1, occupancy θ_T is given by $1 - 1/K\theta_L$ within very good approximation.

In Fig. 8 the trap density N_T is plotted against distance R/b. Density $(N_T)_0 = 8.5 \times 10^{20}$ traps m^{-3} in the undeformed material is used to normalize N_T. The shape of the curve is explained by the fact that the plastic strain $\bar{\varepsilon}^p$ (see Fig. 4) determines the trap populations (see Fig. 8). Near the crack, trap densities are seen to saturate to a distance $R/b = 0.14$. There, plastic strains $\bar{\varepsilon}^p$ are greater than 0.8, the level above which the trap density saturates. Trap densities fall away rapidly beyond the saturation distance $R/b = 0.14$ following the trend of the equivalent plastic strain $\bar{\varepsilon}^p$.

Now, we can explain the shape of the C_T vs R/b curve (Fig. 5) by means of Eq. (3). Values of C_T are in direct proportional relationship to those of N_T since occupancies

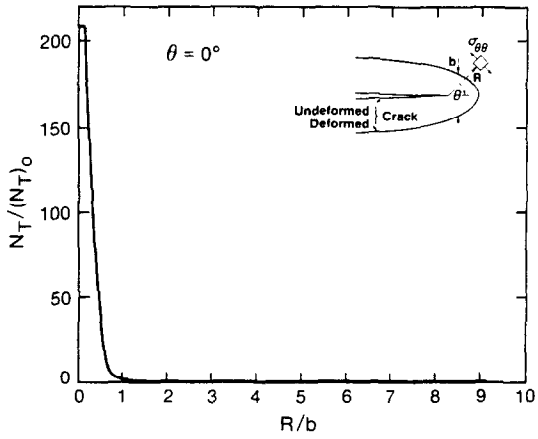

FIG. 8. Plot of the trap density $N_T/(N_T)_0$ vs distance R/b after 130 s when the crack opening displacement b equals $5b_0$. Constant $(N_T)_0$ equals to 8.5×10^{20} traps m^{-3}.

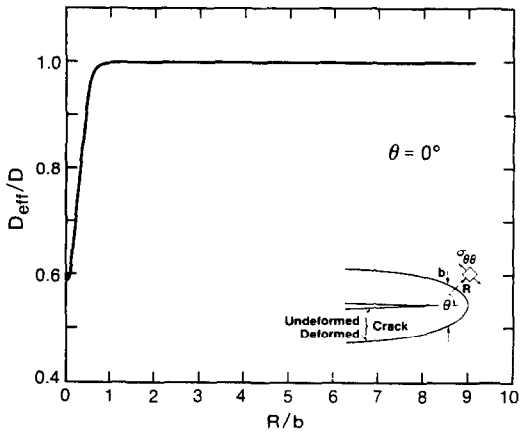

FIG. 9. Plot of the trapping induced effective diffusion constant D_{eff} vs distance R/b for impure iron (σ_0 = 250 MPa) after 130 s when the crack opening displacement b equals $5b_0$. Parameter D is the normal lattice diffusion constant and equals 1.27×10^{-8} m^2 s^{-1}.

θ_T are approximately equal to 1. Therefore, the trap saturated segment $0 \leqslant R/b \leqslant 0.14$ is characterized by the same high concentration values that are about 84.5 times as large as the nominal concentration C_0. Concentration C_H equals the sum $C_L + C_T$ and follows the trends of the dominant concentration C_T.

In Fig. 9, the effective diffusion constant D_{eff} (17) normalized by the normal lattice diffusion constant D is shown vs distance R/b. As we have seen, occupancy θ_T is almost a constant equal to 0.99. Then, (1), (3), (4) and (6) yield the ratio D_{eff}/D mainly inversely dependent on the trap density N_T. Hence, D_{eff}/D is minimal at the notch tip ($R/b = 0$) since N_T is a maximal there. Trap density N_T decreases as R/b increases (see Fig. 8). Consequently D_{eff}/D increases too. However, the density N_T does not vary markedly after a certain distance $R/b = 0.8$. Therefore, the ratio D_{eff}/D behaves in the

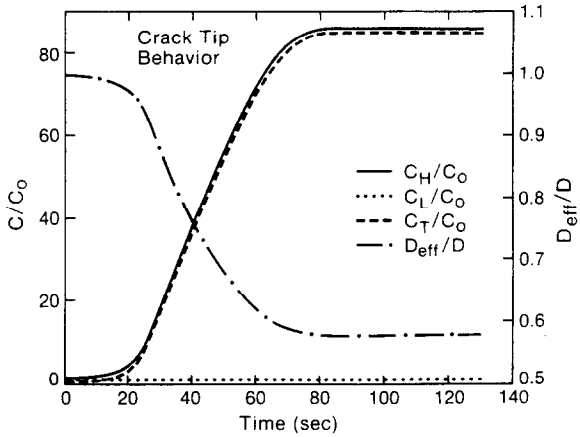

FIG. 10. Evolution in time of notch tip hydrogen concentration C_L/C_0 in NILS, C_T/C_0 in trapping sites, C_H/C_0 ($C_H = C_L + C_T$) and effective diffusion constant D_{eff}/D for impure iron ($\sigma_0 = 250$ MPa).

same way approaching the value of 0.99. Away from the tip trap populations are small and have almost no effect on hydrogen diffusivity.

In Fig. 10 the evolution in time of the quantities C_H, C_L, C_T and D_{eff} on the crack tip is shown as loads are increasing. Obviously, the concentration C_L remains constant since the notch surface concentration is controlled by the boundary condition. The curve representing the trap density N_T vs time, if scaled appropriately, almost coincides with the curve for C_T. Note that the trap density saturates when plastic strains become equal to 0.8 and after 74 s. Also, the concentration C_T and diffusion constant D_{eff} are in agreement with the behavior of N_T as discussed before.

At all times greater than 130 s, loads were held constant. Hydrogen diffusion continues in time under fixed states of plastic strain in the material. A further series of calculations were conducted in order to study the normal lattice diffusion processes since no more trap generation was taking place. At this stage, accurate numerical calculations could be carried out with larger time increments. In Fig. 11, normalized hydrogen concentrations $C_H = C_L + C_T$, C_L and C_T are plotted against R/b after 1419 h and 430 s had elapsed. Variations of concentration C_L with distance are shown more clearly in Fig. 12. The concentration C_L even after 1420 h deviates from that at 130 s by only small amounts. Indeed, the steady state value of C_L throughout the body is well above the initial equilibrium concentration C_0 due to the hydrostatic stress effect. Therefore, the material that extends beyond the tip region as far as 150 mm in the mesh constitutes a sink for NILS hydrogen of enormous capacity. For this reason, the concentrations C_L at points very close to the notch surface do not attain their steady state values within 1420 h despite the rapid diffusion of hydrogen.

(ii) *Results relevant to high strength steels* ($\sigma_0 = 1200$ MPa)

This material was loaded at a rate of 3.3 MPa $\sqrt{m}$ s^{-1} for 47.5 s. The notch was thus blunted to an opening b equal to approximately $5b_0$ at time $t = 47.5$ s. In Fig. 13, the concentration C_L is plotted against R/b at time $t = 47.5$ s. In the same figure,

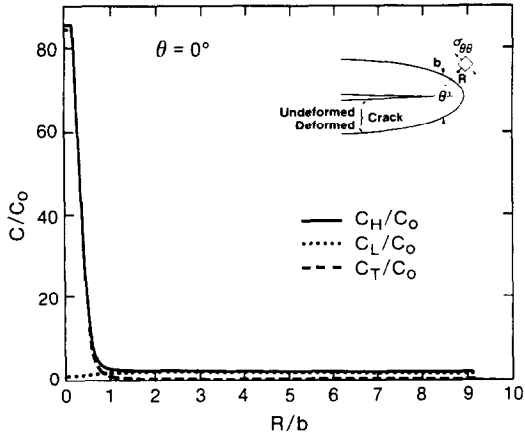

FIG. 11. Plot of hydrogen concentration C_L/C_0 in NILS, C_T/C_0 in trapping sites and C_H/C_0 ($C_H = C_L + C_T$) vs distance R/b for impure iron ($\sigma_0 = 250$ MPa) after 1419 h and 430 s during which the crack opening displacement b was held equal to $5b_0$.

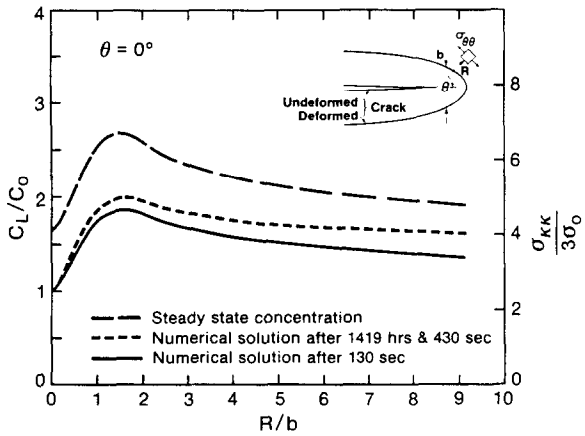

FIG. 12. Plot of hydrogen concentration C_L/C_0 in NILS vs distance R/b for impure iron ($\sigma_0 = 250$ MPa) after 130 s and a further 1419 h and 300 s with the crack opening displacement b held equal to $5b_0$.

the variation of the hydrostatic stress with distance R/b is shown also. Both the peaks of concentration C_L and hydrostatic stress are located at the same distance $R/b = 1.22$ from the notch tip. In the inset of Fig. 13, concentration C_L is replotted against distance R/b along with the corresponding steady state concentration (13). The numerically computed transient values of C_L are much less than those at steady state as was the case in the impure iron. However, the relative difference here is much larger. It is attributable to the stronger competition of the trapping of hydrogen compared to the effect of hydrostatic stress on C_L. This will be discussed further in the next section.

An overwhelming trapping effect is demonstrated in Fig. 14 where the normalized trapping site concentration C_T/C_0 is plotted against distance R/b after 47.5 s. The order of magnitude of concentration C_T can be understood as follows. The nominal concentration C_0 was equal to 2.184×10^{16} hydrogen atoms per m^3 of metal lattice.

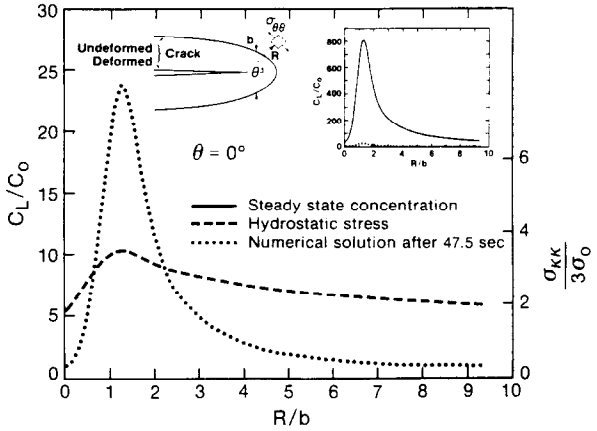

FIG. 13. Plot of hydrogen concentration C_L/C_0 in NILS and hydrostatic stress $\sigma_{kk}/3\sigma_0$ vs distance R/b for high strength steel ($\sigma_0 = 1200$ MPa) after 47.5 s when the crack opening displacement b equals $5b_0$. Concentration C_0 now equals 2.184×10^{16} hydrogen atoms m^{-3}.

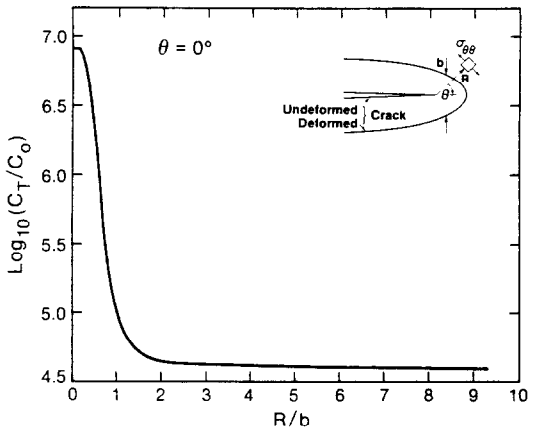

FIG. 14. Plot of hydrogen concentration C_T/C_0 in trapping sites vs distance R/b for high strength steel ($\sigma_0 = 1200$ MPa) after 47.5 s when the crack opening displacement b equals $5b_0$.

From Fig. 13 it is deduced that concentration C_L is less than 5.1848×10^{17} hydrogen atoms per m^3 of metal lattice. Hence, occupancies θ_L are given by (1) to be less than 10^{-12} at temperature $T = 150$ K. Hence $K\theta_L$ is of the order of 10^9. This is a very effective reason for θ_T to be very close to 1 which implies that traps are filled up almost completely all the time. This means that the concentration C_T follows the trap densities N_T directly, as directed by (3). Thus, the concentrations C_T in the steel are of the order of 10^{21} to 10^{23} hydrogen atoms per m^3 of metal lattice in contrast to more modest levels in the iron. Lastly, trap densities N_T and equivalent plastic strains $\bar{\varepsilon}^p$ as functions of distance R/b are of almost the same form as in the case when $\sigma_0 = 250$ MPa (see Figs 8 and 4). This is because the material was strained to the same final crack opening displacement and the trap generation process was assumed to be the same in both materials.

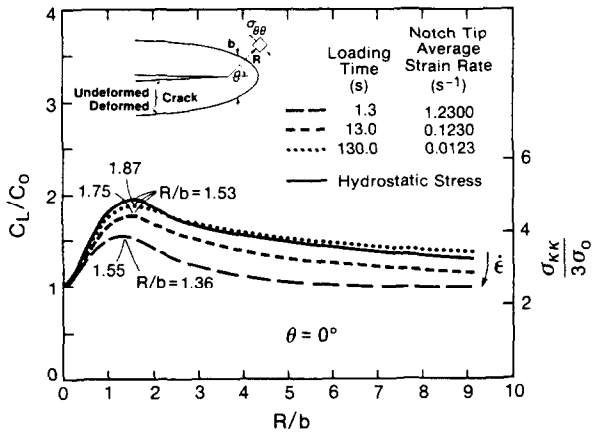

FIG. 15. Plot of hydrostatic stress $\sigma_{kk}/3\sigma_0$ and hydrogen concentration C_L/C_0 in NILS vs distance R/b for impure iron ($\sigma_0 = 250$ MPa) when the crack opening displacement b equals $5b_0$ under various loading rates. Concentration C_0 equals 2.084×10^{21} hydrogen atoms m^{-3}.

(iii) *Results concerning the effect of strain rate*

The effect of strain rate on the hydrogen population development was studied by shortening the time interval during which the loads were applied. The numerical calculations carried out were relevant to the impure iron case ($\sigma_0 = 250$ MPa). The material was loaded up to the same level, namely the crack was blunted to 5 times its initial width ($b = 5b_0$). However, this was achieved after 13 s in one case and 1.3 s in another.

The average strain rate that the notch tip surface experienced in the previous calculations for impure iron was 0.0123 s^{-1}. Now, by increasing the loading rate, we forced the notch tip to experience average strain rates of 0.123 and 1.23 s^{-1} respectively. These strain rates are well below the critical strain rate at which a hydrogen atmosphere breaks away from a dislocation. TIEN *et al.* (1976) define this critical rate in iron alloys as $10^{-7}\rho_H$ cm^2 s^{-1} where ρ_H is the density of the hydrogen-carrying dislocations. Thus, the smallest critical strain rate is for annealed iron and equals 10 s^{-1} when the dislocation density is taken equal to 10^8 lines per cm^2.

In Fig. 15, the normalized NILS concentration C_L is plotted against distance R/b ahead of the notch tip for various strain rates. The crack opening displacement b has just reached $5b_0$ in all cases. We see immediately that the higher the strain rate, the lower the resulting concentration C_L. When the strain rate becomes sufficiently high, the peak of the concentration C_L does not coincide any longer with that of the hydrostatic stress. Rather, it shifts towards the notch tip. These effects are explained by the notion that higher strain rates correspond to faster trap generation and hydrogen trapping compared to lattice diffusion rates. Hence, the higher the strain rate, the faster is the preferential motion of hydrogen to traps near the notch tip. As a result, hydrogen is depleted from the lattice and less is available to be distributed according to concentration gradient and hydrostatic stress induced diffusion. In the case when the strain rate was 1.23 s^{-1}, hydrogen accumulated so close to, and so quickly at, the tip that the hydrostatic stress peak at $R/b = 1.53$ was not able to pull hydrogen to it and establish a concentration peak at $R/b = 1.53$.

6. DISCUSSION OF THE RESULTS

The results reported in the preceding section indicate that there are two competing mechanisms influencing the distribution of hydrogen near a crack tip. One is the traps generated by plastic straining (concentration C_T) and the other is the tensile hydrostatic stress (concentration C_L). Hydrogen accumulates mainly in traps as long as plastic straining continuously generates them (see Figs 5, 8 and 14). The site of accumulation of trapped hydrogen is near the crack surface as dictated by plasticity (see Figs 4 and 8). Its extent depends on the distance from the crack surface over which plastic strains are of the order of 0.8. In contrast, the NILS concentration C_L is only mildly elevated at the peak of the hydrostatic stress $\frac{1}{3}\sigma_{kk}$ at this stage in which straining has just ceased (see Figs 6 and 13). This reflects the fact that traps pull hydrogen away from the NILS. This influence overrides the competing hydrostatic stress effect that induces hydrogen to reside at NILS in high triaxiality regions some distance from the crack surface (see Figs 6 and 13). For example when the crack opening displacement b has just reached $5b_0$ in the impure iron case, Fig. 5 shows that the maximum trapping site concentration C_T is 85.6 times as large as the nominal concentration C_0. On the other hand, Fig. 6 shows that the maximum NILS concentration C_L is only 1.87 times as large as C_0. Similarly, when the crack opening displacement has just reached $5b_0$ in the high strength steels case, Fig. 14 shows a trapping site concentration C_T in the saturation region near the crack tip equal to 8.14×10^6 times the nominal concentration C_0. In contrast, Fig. 13 indicates that the NILS concentration C_L, at a maximum, is only 24 times larger than C_0 at this stage.

The transient effects of diffusion during straining are very significant in the competition for hydrogen between regions of high hydrostatic stress and regions of high trap density. After plastic straining ceases and traps are no longer being created, diffusion processes will then start to deliver hydrogen to NILS in areas of high hydrostatic stress which have not reached the steady state level determined by that stress. In contrast, there will be little further change in the trapped concentration of hydrogen after plastic straining terminates since the density of traps' sites is constant thereafter. Furthermore in the high hydrostatic stress region, the plastic strain and therefore the density of traps is low. As a result, most of the hydrogen there resides in the lattice. Equilibrium between the traps and the lattice dictates that the preponderance of hydrogen arriving at the high hydrostatic stress location remains in the lattice and only a small amount enters the traps. For example, in the *case of iron*, plastic straining ceases after 130 s. Figure 11 indicates that the trapping site concentration C_T at time $t \simeq 1420$ h is almost identical to that at time $t = 130$ s (see Fig. 5). On the other hand, Fig. 12 shows that the hydrostatic stress effect beyond the high trap density region ($R/b > 0.8$) is drawing hydrogen towards that location. Beyond there, the demand for trap filling hydrogen has fallen almost to zero. The reason for the small change to the NILS concentration after 1420 h is the large volume of material around the crack. Effectively, the body in question has a diameter of approximately 300 mm and so there is an enormous amount of material to fill with hydrogen. This is a drawback to the plane strain small scale yielding approach adopted for this problem since the diffusion distances are specified by the size of the domain analysed. No allowance is made for the location of the physical boundaries of the

body either in plane or out of plane and the results can be misleading as a consequence. However, the calculations do show that it would take very long times for steady state hydrogen distributions to be achieved in large bodies containing cracks.

If the calculations were carried out for smaller bodies, the approach to steady state distributions of hydrogen would occur faster. However, after the steady state is achieved the lattice concentration C_L close to the crack surface would still be negligible compared with the concentration in traps C_T in the same element of material. Of course, at the location of the peak hydrostatic stress, the resulting steady state value of C_L would be larger than C_T but it would still be very small compared to the concentration C_T prevailing in the trap saturation region on the crack surface. Consequently the regions of high hydrogen concentration are still determined predominantly by the plastic strain because of its role in creating traps. This distribution very near the crack tip would be very similar to that shown in Fig. 5.

In view of this, the hydrogen distribution near blunt cracks can be estimated from a knowledge of the relationship between the trap density and the plastic strain and from the distribution of plastic strain ahead of the crack as shown in Fig. 4. If the curve of Fig. 1 for trap density against $\bar{\varepsilon}^p$ was steeper, one would expect higher values of C_T spread over much larger distances from the crack surface. On the other hand, if the slope of the curve was low with large values of N_T only at extremely high plastic strains, one would expect high concentrations of C_T only very near the crack surface. Finally, a uniform concentration would be established if the trap densities were plastic strain independent.

Another aspect of the results can be deduced from the insignificant nature of the contribution from the NILS concentration, as illustrated in Figs 11 and 12. This is the reason why the results of our calculations are boundary condition independent. In other words, it does not matter whether hydrogen can enter the intensely deformed region ahead of the crack through the crack surface or arrives by bulk lattice diffusion processes from the far field. The lattice diffusion delivers the hydrogen, but the existence of traps determines the distribution. Therefore, our results confirm the thesis of VENNETT and ANSELL (1967) that the contribution of lattice diffusion in determining the hydrogen distribution is unimportant.

The conclusions drawn so far are endorsed by the results for *high strength steels* (see Figs 13 and 14). The fact that high strength steels suffer severely from embrittlement raises the question of whether hydrostatic stress effects are more significant in these materials. Indeed, the hydrostatic stress may become equal to 4176 MPa (see Fig. 13) in these systems. This value is far larger than that in the case of impure iron (1230 MPa). However, the results for high strength steel are qualitatively similar to those for iron. Although the NILS concentration of hydrogen is pronounced in the high hydrostatic stress region in our results, it is far below the steady state concentration that would eventually prevail in the hydrostatic stress peak location. The latter, exponentially dependent on the hydrostatic stress, is 810 times the nominal concentration C_0 (see Fig. 13) when the crack opening displacement is equal to 5 times the initial one. In contrast, the transient value when this blunting level has just been achieved is 24 C_0. Moreover, even if the steady state values of C_L were achieved more rapidly than in our calculations, as they would be in a body of smaller size, C_L would still be negligible when compared to the large trapping site concentrations very

close to the crack surface (see Figs 13 and 14). Again, the conclusion is that trapping plays an important role in attracting hydrogen. Hydrostatic stress effects are less important as far as location and magnitude of the total hydrogen concentrations are concerned.

Concerning the results for the *effect of strain rate*, the trapped hydrogen population is unaffected. At low strain rates, hydrogen can diffuse rapidly relative to the rate at which traps are created. Consequently, traps can be filled readily and the lattice concentration maintained. In that case, more hydrogen can accumulate in highly stressed areas as hydrostatic stress dictates. As a result, the concentration C_L is more pronounced about the hydrostatic stress peak at the lower strain rates (see Fig. 15). At high loading rates,the NILS diffusion is too slow to supply the traps in the high plastic strain region which exert an attraction for hydrogen. The traps are filled from the lattice nearby and this has the effect of depleting the lattice and diminishing the relative hydrogen concentration in the high hydrostatic stress region. In Fig. 15 the maximum of concentration C_L has moved toward the crack surface at $\dot{\varepsilon} = 1.23\ s^{-1}$. Also, it is lower than that at $\dot{\varepsilon} = 0.0123\ s^{-1}$. However, we note that the maximum NILS hydrogen population is generally negligible compared with the maximum trapping site concentration and so this particular effect of strain may be unimportant in processes causing hydrogen failures if it is the trapped hydrogen which is important.

It should be noted that temperature is an important factor in the interaction between the competing mechanisms of storage of hydrogen in the lattice and in the traps. As noted in the previous section, when C_L is fixed, an increase of temperature diminishes both the hydrogen atoms that enter traps and the effect of tensile hydrostatic stress in attracting hydrogen. Increased temperature also reduces the flow stress, so the tensile hydrostatic stress in front of a crack is diminished also. These effects will be present in both the transient hydrogen diffusion and in the steady state distribution. Since we have no transient results for different temperatures, the effect will be discussed as it affects the steady state. The steady state value of C_L due to the effect of hydrostatic stress can be obtained through (13) while the trapping site concentration C_T associated with a nominal NILS concentration can be deduced from (7).

At 300 K and at typical stress levels ahead of cracks ($\sigma_{kk}/3\sigma_0 \simeq 2.5$) there is a negligible elevation of the lattice concentration in low strength irons. In comparison, at plastic strains of order unity which prevail around blunt cracks, the trapped concentration can be as large as 10 times the nominal lattice value. Hence, at 300 K, there is only one order of magnitude difference at most in the maxima of the two types of concentration prevailing in steady state. The difference is even less significant in the high strength steels at 300 K, where the lattice concentration is elevated by stress to about 10 times the nominal lattice value and the trapped concentration maximum is about the same. Thus, at room temperature, there is no marked difference in the largest concentrations associated with the two mechanisms of storage in both types of alloy. However, at low temperatures, $T < 200$ K, and at strains of order unity around a blunt crack, the trapped concentrations can be several orders of magnitude larger than the nominal lattice concentration in both types of alloy. In contrast, the hydrostatic stress ahead of the crack increases the lattice concentration only about one hundredfold in the case of high strength steel and by an amount of order unity in low strength iron alloys. Thus at these lower temperatures, there is a tendency

for trapping to overwhelm lattice concentrations as far as the maximum levels are concerned. This is apparent in the transient calculations presented previously for high strength steel. The computations are based on the use of material parameters relevant to that alloy at 150 K. In contrast, the results for iron pertain to a temperature of 300 K.

7. Implications for Fracture

At this stage we can try to draw some rather general conclusions from our results concerning embrittlement fractures in steels and iron of the type characterized in our calculations. If fracture is induced purely by a critical hydrogen concentration, then it is likely that it will occur on or very close to the blunt crack surface. We draw this conclusion because of the very high trapping site hydrogen concentration near the blunt crack. Also involved is an assumption that the lattice hydrogen concentrations alone are not the issue because those concentrations are quite unexceptional, especially compared to the maximum trapping site concentrations. Thus we would expect to see the initiation of failure taking place very close to the crack tip, as opposed to initiating at the high hydrostatic stress region 2 crack openings ahead of the tip.

The evidence is that trap density saturates after a certain level of plastic strain, and so around the blunt crack tip there is a region of saturated concentration of trapped hydrogen. At this stage, failure cannot be caused by concentration alone, since it no longer increases as straining continues. Thus, the concept of a critical size in which the failure process operates must be introduced similar to criteria used in ductile fracture (McClintock, 1958). This idea is that the region of saturated trapped hydrogen must spread over a critical material distance before failure can be initiated. The size of the saturated zone is proportional to the current crack opening displacement. In consequence, the failure will initiate when the crack opening displacement reaches a critical level. This in turn can be translated into a critical value of the J-integral (Rice, 1968a) or a critical value of the stress intensity factor.

Moreover, the evidence is that hydrogen concentration combined with other contributing factors determines the critical state for fracture. For example, Tabata and Birnbaum (1983, 1984) and Robertson and Birnbaum (1986) have found that hydrogen enhances dislocation mobility and multiplication rates and this can cause crack propagation through highly localized plasticity at a crack tip in pure iron. Lee *et al.* (1977, 1979a) and Onyewuenyi and Hirth (1983) identified the role of hydrogen in promoting plastic instability that leads to crack initiation at the crack surface in the spheroidized AISI 1090 and 1095 steels. Furthermore, they comment that surface crack initiation was not affected by internal stress triaxiality. Interestingly enough Lee *et al.* (1979b) have found that hydrogen may cause internal microcracking in tempered AISI 4340 steel but definitely not in the high stress region. Since the steel used had a high yield stress (1280 MPa), the stress concentration away from the tip may have played a synergistic role with the effect of hydrogen alone in nucleating microcracking. Similar observation is made in the work by Costa and Thompson (1982) in the case of pearlitic 1045 steel.

On the other hand, our results can be used in combination with any criterion proposed for hydrogen embrittlement. A reservation is that the glacial approach to steady state in our calculations for a very large body makes it impossible to test criteria against the observed behavior of small or thin specimens. Our results show the following combination on the line ahead of a blunt crack tip: falling hydrogen concentration and plastic strain level and a rising stress level. Thus, a process of failure which operates when some combined level of hydrogen concentration, plastic strain level and stress level is reached will function when the critical condition are achieved somewhere between the crack tip and the point where the stress level peak lies, i.e. 2 crack openings ahead of the tip. For example, in the decohesion model of hydrogen induced rupture, the stress to fail grain boundaries is reduced by the presence of hydrogen with larger concentrations of hydrogen causing greater reductions of failure stress. Thus, the critical combination of conditions might be met not on the crack surface where there is most hydrogen and least stress but further in from the crack where there is more stress. That is not to say that decohesion is the model for hydrogen induced rupture that we prefer. However, the example illustrates how fracture mechanisms might occur in the interior of the material ahead of the crack.

Ductile modes of failure are known to function in many alloys subject to embrittlement. It is possible that the mechanism of this hydrogen induced fracture in some cases is localized plastic shear leading to rupture. Two possible causes can be suggested. One is softening and enhanced dislocation motion directly caused by the presence of hydrogen and this will be discussed in a future paper. Another cause could be easy nucleation of voids from inclusions due to the trapped hydrogen on the interface. This can cause plastic softening effectively and in turn led to plastic flow localization (RICE, 1977a). The decohesion mechanism would operate at the level of the interface between inclusions and matrix. Thus, the previous comments concerning the combined effect of hydrogen and stress pertain and the failure would initiate by void nucleation induced localization somewhere between the crack tip and the hydrostatic stress peak. That is, if considerable reduction of cohesion is caused by hydrogen, localization and shear rupture would occur at the crack surface where there is most strain. If modest reduction of cohesion is induced by the hydrogen, then it would be expected that failure would initiate closer to the hydrostatic stress peak.

If localization is not the mechanism leading to ductile fracture, then void nucleation, growth and coalescence can be suggested as the standard process of failure. Void nucleation could be affected by hydrogen in the manner discussed above. Growth and coalescence might be enhanced by softening due to hydrogen, and this will be discussed in a future publication. Thus, without softening, void controlled fracture would occur by the combined effect of hydrogen and stress influencing nucleation and hydrostatic stress and plastic strain influencing growth and coalescence. This would seem to indicate a process taking place somewhere between the crack tip and the hydrostatic stress peak. The question of the brittle nature of the failure must be squared with the above classical ductile fracture model for hydrogen induced fracture. An explanation might lie in the possibility of large reductions in cohesion leading to the local nucleation of a very large density of voids. These voids would not have to grow much before coalescence, leading to brittle-like fracture at low strains. Another possibility is that the hydrogen concentrates more in a zone in the vicinity of the grain boundaries,

confining void nucleation and softening, if present, to that location (ROBERTSON and BIRNBAUM, 1986).

The discussion above is a broadly drawn overview of mechanisms that could be modeled more extensively as a consequence of the numerical results described in this paper. Another possibility is that these mechanisms would be incorporated into the numerical modeling in future work to investigate the detailed behavior as a possible explanation of different types of hydrogen embrittlement. It should be noted that we have assumed a homogeneous isotropic distribution of traps. Their density at any point reflected the local plastic strain. Any locally oriented planar traps such as grain boundaries were not accounted for in this formulation although cracking may favor such traps or line and point traps in planar array. An improved version of the theory would allow for such features.

In addition, the numerical methods we have developed could be used to model macroscopic experiments such as fracture toughness tests. By systematically varying parameters which are possibly important in the embrittlement behavior and comparing the experimental results with equivalent numerical solutions, one could critically investigate the relative importance of such features as trapped hydrogen, lattice hydrogen, transient distributions and steady state distributions. This is so because relative amounts of lattice and trapped hydrogen as the test evolves can be adjusted by varying temperature, specimen, size, strain ratio and prior plastic work in the experiments and in the accompanying calculations. Thus, we believe that our numerical results and methods have and can in future shed light on the phenomenon of hydrogen embrittlement.

8. CLOSURE

Hydrogen transport coupled with large deformation elastic–plastic analysis has been studied in the vicinity of a blunting crack tip in iron systems. The numerical results show that during plastic straining hydrogen accumulates mainly in traps near the crack surface. On the other hand, the hydrogen concentration at normal interstitial lattice sites is only mildly elevated at the peak site of the hydrostatic stress in the material near the notch. Therefore, the areas of high hydrogen concentration are determined predominantly by the plastic strain, because of its role in creating traps. This picture still prevails after plastic straining terminates and steady state conditions are established. Consequently, lattice diffusion delivers the hydrogen but the existence of trapping determines the distribution. As a result, the role of stress triaxiality in determining the sites of hydrogen accumulation is not as important as once believed. The strain rate effect has been treated with regard to its effect on the trap generation rates. In that respect, it is unimportant to hydrogen failures because the final amount of hydrogen concentration is not affected. This is despite the fact that lattice concentrations reduce as the loading rate becomes higher. The predominant trapped hydrogen populations are the same and independent of loading rate. The temperature effect on the equilibrium between lattice and trapped hydrogen has been discussed also under steady state conditions. At low temperatures and large plastic straining hydrogen overwhelmingly resides in the traps.

The situation ahead of a crack tip is that of strain and total hydrogen concentration diminishing with distance from the crack tip on the one hand, and rising triaxiality on the other. Thus, fractures characterized by critical hydrogen concentration alone would initiate very close to the crack tip rather than at the hydrostatic stress peak site. If failure is not induced by concentration alone, then, a critical combination of stress, strain and concentration may be considered as the initiation criterion. In this way, failures are expected to commence somewhere between the crack tip and the site of the triaxiality peak. Thus, the notion of a "critical length" in the fracture phenomenon is alluded to. In this context, possible brittle and ductile modes of failure are outlined and their initiation sites are identified. The significance of the numerical methods and results in modeling macroscopic experiments is emphasized. Furthermore, failure mechanisms can be employed in future work in the numerical modeling in order to explain the various types of hydrogen embrittlement.

ACKNOWLEDGEMENTS

The authors are indebted to Professor H. K. BIRNBAUM for suggesting the topic in this paper and for providing invaluable advice during the development of the research. In addition, the research was supported by the Department of Energy through contract DE-AC02-76ER01198 with the Materials Research Laboratory at the University of Illinois at Urbana-Champaign.

REFERENCES

ADAIR, A. M. 1966 *Trans. Met. Soc. AIME* **236,** 1613.

ALLEN-BOOTH, D. M., ATKINSON, C. and BILBY, B. A. 1975 *Acta Metall.* **23,** 371.

ASANO, S. and OTSUKA, R. 1976 *Scripta Metall.* **10,** 1015.

ASANO, S. and OTSUKA R. 1978 *Scripta Metall.* **12,** 287.

BEACHEM, C. D. 1972 *Metall. Trans.* **3,** 437.

BEACHEM, C. D. 1977 *Stress Corrosion Cracking and Hydrogen Embrittlement of Iron Base Alloys*, NACE-5, p. 376 (edited by R. W. STAEHLE, J. HOCHMANN, R. D. MCCRIGHT and J. E. SLATER), NACE, Texas.

BERNSTEIN, I. M. 1974 *Scripta Metall.* **8,** 343.

BERNSTEIN, I. M. and THOMPSON, A. W. 1976 *Int. Metals Rev.* **21,** 269.

BIRNBAUM, H. K. 1979 *Environmental Sensitive Fracture of Engineering Materials* (Proc. Symp. Environmental Effects on Fracture, Chicago, Illinois, October 24–36, 1977), p. 326 (edited by Z. A. FOROULIS), Metallurgical Society of AIME, Warrendale, Pennsylvania.

BIRNBAUM, H. K. 1983 *Atomistics of Fracture* (Proc. NATO Advanced Research Institute on Atomistics of Fracture, Calcatoggio, Corsica, France, May 22–31, 1981), p. 733 (edited by R. M. LATANISION and J. R. PICKENS), Plenum Press, New York.

BIRNBAUM, H. K.	1984	*Hydrogen Embrittlement and Stress Corrosion Cracking* (Proc. Troiano Festschrift Symposium, Case Western Reserve University, June 1–3, 1980), p. 153 (edited by R. GIBALA and R. F. HEHEMANN), ASM, Ohio.
BIRNBAUM, H. K.	1985	Unpublished report.
COSTA, J. E. and THOMPSON, A. W.	1982	*Metall. Trans.* **13A**, 1315.
CULHAM, W. E. and VARGA, R. S.	1971	*J. Soc. Petrol. Engng* p. 374.
DONOVAN, J. A.	1976a	*Metall. Trans.* **7A**, 145.
DONOVAN, J. A.	1976b	*Metall. Trans.* **7A**, 1677.
EASTMAN, J., HEUBAUM, F., MATSUMOTO, T. and BIRNBAUM, H. K.	1982	*Acta Metall.* **30**, 1579.
EASTMAN, J., MATSUMOTO, T., NARITA, N., HEUBAUM, F. and BIRNBAUM, H. F.	1981	*Hydrogen in Metals*, p. 397 (edited by I. M. BERNSTEIN and A. W. THOMPSON), Metallurgical Society of AIME, New York.
ELLERBROCK, H.-G. VON, VIBRANS, G. and STÜWE, H.-P.	1972	*Acta Metall.* **20**, 53.
FRANKEL, G. S. and LATANISION, R. M.	1986	*Metall. Trans.* **17A**, 861.
GARBER, R., BERNSTEIN, I. M. and THOMPSON, A. W.	1976	*Scripta Metall.* **10**, 341.
GARBER, R., BERNSTEIN, I. M. and THOMPSON, A. W.	1981	*Metall. Trans.* **12A**, 225.
GERBERICH, W. W.	1974	*Hydrogen in Metals*, p. 115 (edited by I. M. BERNSTEIN and A. W. THOMPSON), ASM, Ohio.
GERBERICH, W. W., CHEN, Y. T. and JOHN, C. St.	1974	*Metall. Trans.* **6A**, 1485.
GERBERICH, W. W., GARRY, J. and LESSAR, J. F.	1976	*Effects of Hydrogen on Behavior of Materials*, p. 71 (edited by A. W. THOMPSON and I. M. BERNSTEIN), Metallurgical Society of AIME, New York.
GERBERICH, W. W., LIVNE, T. and CHEN, X.-F.	1987	*Chemistry and Physics of Fracture* (edited by R. M. LATANISION and R. H. JONES), Martinus Nijhoff, Dordrecht.
HIRTH, J. P.	1977	*Stress Corrosion Cracking and Hydrogen Embrittlement of Iron Base Alloys*, NACE 5, p. 1 (edited by R. W. STAEHLE, J. HOCHMANN, R. D. MCCRIGHT and J. E. SLATER), NACE, Texas.
HIRTH, J. P.	1980	*Metall. Trans.* **11A**, 861.
HIRTH, J. P.	1984	*Hydrogen Embrittlement and Stress Corrosion Cracking* (Proc. Troiano Festschrift Symposium, Case Western Reserve University, June 1–3, 1980), p. 29 (edited by R. GIBALA and R. F. HEHEMANN), ASM, Ohio.
HIRTH, J. P. and RICE, J. R.	1980	*Metall. Trans.* **11A**, 1501.
IRWIN, G. R.	1960	*Structural Mechanics* (Proc. First Symp. Naval Structural Mechanics, Stanford, 1959), p. 557 (edited by J. N. GOODIER and N. J. HOFF), Pergamon Press, London.
JOHNSON, H. H.	1974	*Hydrogen in Metals*, p. 35 (edited by I. M. BERNSTEIN and A. W. THOMPSON), ASM, Ohio.

JOHNSON, H. H. 1984 *Hydrogen Embrittlement and Stress Corrosion Cracking* (Proc. Troiano Festschrift Symposium, Case Western Reserve University, June 1–3, 1980), p. 3 (edited by R. GIBALA and R. F. HEHEMANN), ASM, Ohio.

JOHNSON, H. H., MORLET, J. G. and TROIANO, A. R. 1958 *Trans. Met. Soc. AIME* **212**, 528.

KEDZIERZAWSKI, P. 1985 *Hydrogen Degradation of Ferrous Alloys*, p. 251 (edited by R. A. ORIANI, J. P. HIRTH and M. SMIALOWSKI), Noyes Publications, New Jersey.

KIMURA, H., MATSUI, H., KIMURA, A., KIMURA, T. and OGURI, K. 1981 *Hydrogen in Metals*, p. 191 (edited by I. M. BERNSTEIN and A. W. THOMPSON), Metallurgical Society of AIME, New York.

KITAGAWA, H. and KOJIMA, Y. 1983 *Atomistics of Fracture* (Proc. NATO Advanced Research Institute on Atomistics of Fracture, Calcatoggio, Corsica, France, May 22–31, 1981), p. 799 (edited by R. M. LATANISION and J. R. PICKENS), Plenum Press, New York.

KUMNICK, A. J. and JOHNSON, H. H. 1980 *Acta Metall.* **28**, 33.

KURKELA, M. and LATANISION, R. M. 1979 *Scripta Metall.* **13**, 927.

LADNA, B. and BIRNBAUM, H. K. 1987 *Acta Metall.* **35**, 1775.

LATANISION, R. M. 1983 *Atomistics of Fracture* (Proc. NATO Advanced Research Institute on Atomistics of Fracture, Calcatoggio, Corsica, France, May 22–31, 1982), p. 3 (edited by R. M. LATANISION and J. R. PICKENS), Plenum Press, New York.

LEE, H. M. 1976 *Metall. Trans.* **7A**, 431.

LEE, T. D., GOLDENBERG, T. and HIRTH J. P. 1977 *Fracture 1977* (Proc. Fourth Int. Conf. Fracture, Waterloo, Canada, June 1977), Vol. 2, p. 243 (edited by D. M. R. TAPLIN), Pergamon, Oxford.

LEE, T. D., GOLDENBERG, T. and HIRTH, J. P. 1979a *Metall. Trans.* **10A**, 199.

LEE, T. D., GOLDENBERG, T. and HIRTH, J. P. 1979b *Metall. Trans.* **10A**, 439.

LI, J. C. M., ORIANI, R. A. and DARKEN, L. S. 1966 *Z. Physik. Chem. Neue Folge* **49**, 271.

LIU, H. W. 1970 *Trans. ASME J. Basic Engng* **92**, 633.

MATSUI, H., KIMURA, H. and KIMURA, A. 1979 *Mat. Sci. Engng* **40**, 227.

MATSUI, H., KIMURA, H. and MORIYA, S. 1979 *Mat. Sci. Engng* **40**, 207.

MATSUMOTO, T., EASTMAN, J. and BIRNBAUM, H. K. 1981 *Scripta Metall.* **15**, 1033.

MATSUYAMA, S., PLUSQUELLEC, J., AZOU, P. and BASTEIN, P. 1978 *Hydrogen in Metals* (Proc. 2nd Int. Cong., Paris, France, June 6–10, 1977), Vol. 3, p. 3A2 **1**, Pergamon Press, New York.

MCCLINTOCK, F. A. 1958 *J. appl. Mech.* **25**, 582.

MCMEEKING, R. M. 1977 *J. Mech. Phys. Solids* **25**, 357.

MCMEEKING, R. M. and RICE, J. R. 1975 *Int. J. Solids Struct.* **11**, 601.

MCNABB, A. and FOSTER, P. K. 1963 *Trans. Met. Soc. AIME* **227**, 618.

METALS HANDBOOK	1985	Edited by H. E. BOYER and T. L. GALL, ASM, Ohio.
MORGAN, M. J. and MCMAHON, C. J.	1985	*Hydrogen Degradation of Ferrous Alloys*, p. 608 (edited by R. A. ORIANI, J. P. HIRTH and M. SMIALOWSKI), Noyes Publications, New Jersey.
MORIYA, S., MATSUI, H. and KIMURA, H.	1979	*Mat. Sci. Engng* **40**, 217.
NAGTEGAAL, J. C., PARKS, D. M. and RICE, J. R.	1974	*Comp. Meth. appl. Mech. Engng* **4**, 153.
NELSON, H. G.	1983	*Treatise on Materials Science and Technology, Embrittlement of Engineering Alloys*, Vol. 25, p. 275 (edited by C. L. BRIANT and S. K. BANERJI), Academic Press, New York.
OGURI, K. and KIMURA, H.	1980	*Scripta Metall.* **14**, 1017.
ONYEWUENYI, O. A. and HIRTH, J. P.	1983	*Metall. Trans.* **14A**, 259.
ORIANI, R. A.	1969	*Fundamental Aspects of Stress Corrosion Cracking*, NACE-1, p. 32 (edited by R. W. STAEHLE, A. J. FORTY and D. VANROOYEN), NACE, Texas.
ORIANI, R. A.	1970	*Acta Metall.* **18**, 147.
ORIANI, R. A.	1978	*Ann. Rev. Mater. Sci.* **8**, 327.
ORIANI, R. A.	1983	*Atomistics of Fracture* (Proc. NATO Advanced Research Institute on Atomistics of Fracture, Calcatoggio, Corsica, France, May 22–31, 1982), p. 795 (edited by R. M. LATANISION and J. R. PICKENS), Plenum Press, New York.
ORIANI, R. A. and JOSEPHIC, P. H.	1974	*Acta Metall.* **22**, 1065.
ORIANI, R. A. and JOSEPHIC, P. H.	1977	*Acta Metall.* **25**, 979.
ORTIZ, M. and POPOV, E. P.	1985	*Int. J. Num. Meth. Engng* **21**, 1561.
PIERCY, G. R.	1978	*Met. Soc. CIM Annual Vol.* **16**, 11.
RICE, J. R.	1968a	*J. appl. Mech.* **35**, 379.
RICE, J. R.	1968b	*Fracture: An Advanced Treatise*, Vol. 2, p. 191 (edited by H. LIEBOWITZ), Academic Press, New York.
RICE, J. R.	1976	*Corrosion* **32**, 22.
RICE, J. R.	1977a	*Theoretical and Applied Mechanics* (Proc. 14th IUTAM Congress, Delft, The Netherlands, August 30–September 4, 1976), p. 207 (edited by W. T. KOITER), North Holland, Amsterdam.
RICE, J. R.	1977b	*Stress Corrosion Cracking and Hydrogen Embrittlement of Iron Base Alloys*, NACE-5, p. 11 (edited by R. W. STAEHLE, N. J. HOCHMANN, R. D. MCCRIGHT and J. E. SLATER), NACE, Texas.
ROBERTSON, I. M. and BIRNBAUM, H. K.	1986	*Acta Metall.* **34**, 353.
SAKAMOTO, Y., BABA, K. and SUEHIRO, T.	1985	*Scripta Metall.* **19**, 871.
SMIALOWSKI, M.	1985	*Hydrogen Degradation of Ferrous Alloys*, p. 561 (edited by R. A. ORIANI, J. P. HIRTH and M. SMIALOWSKI), Noyes Publications, New Jersey.
SOFRONIS, P.	1987	Ph.D. Thesis, University of Illinois at Urbana-Champaign, Urbana, Illinois.

STEIGERWALD, E. A., SCHALLER, F. W. and TROIANO, A. R. 1960 *Trans. Met. Soc. AIME* **218**, 832.

STURGES, C. M. and MIODOWNIK, A. P. 1969 *Acta Metall.* **17**, 1197.

TABATA, T. and BIRNBAUM, H. K. 1983 *Scripta Metall.* **17**, 947.

TABATA, T. and BIRNBAUM, H. K. 1984 *Scripta Metall.* **18**, 231.

TIEN, J. K., THOMPSON, A. W., BERNSTEIN, I. M. and RICHARDS, R. J. 1976 *Metall. Trans.* **7A**, 821.

TROIANO, A. R. 1960 *Trans. ASM* **52**, 54.

VAN LEEUWEN, H. P. 1974 *Engng Fracture Mech.* **6**, 141.

VAN LEEUWEN, H. P. 1976 *Effect of Hydrogen on Behavior of Materials*, p. 480 (edited by A. W. THOMPSON and I. M. BERNSTEIN), Metallurgical Society of AIME, New York.

VENNETT, R. M. and ANSELL, G. S. 1967 *Trans. ASM* **60**, 242.

VÖLKL, J. and ALEFELD, G. 1978 *Hydrogen in Metals, Topics in Applied Physics*, Vol. 28, p. 321 (edited by G. ALEFELD and J. VÖLKL), Springer, Berlin, Heidelberg.

WANG, Y. B., CHU, W. Y. and HSIAO, C. M. 1985 *Scripta Metall.* **19**, 1161.

WERT, C. A. 1978 *Hydrogen in Metals, Topics in Applied Physics*, Vol. 28, p. 305 (edited by G. ALEFELD and J. VÖLKL), Springer, Berlin, Heidelberg.

ZIENKIEWICZ, O. C. 1977 *The Finite Element Method*, McGraw-Hill, London.